MAGNETOHYDRODYNAMICS Vol. 42 (2006), No. 2-3, pp. 225–236

CURRENT APPROACHES TO MODELING MHD FLOWS IN THE DUAL COOLANT LEAD LITHIUM BLANKET

S. Smolentsev[1], *N.B. Morley*[1], *M. Abdou*[1], *R. Munipalli*[2], *R. Moreau*[3]

[1] *UCLA, 43-133 Engineering IV, Box 951597, Los Angeles, CA 90095-1597, USA*
[2] *HyPerComp, 31255 Cedar Valley Drive, Westlake Village, CA 91362-7140, USA*
[3] *EPM Laboratory, ENSHM de Grenoble, BP 95, 38402 St Martin d'Hères Cedex, France*

The ongoing work on the development of modeling tools to address MHD flows in the Dual Coolant Lead Lithium blanket has been presented. Analysis is performed for rectangular channel flows with a SiC_f/SiC flow channel insert in a toroidal magnetic field. Such effects as 2D turbulence and buoyancy are considered. A newly-developed 3D MHD software HIMAG is described, which is potentially an effective tool to study complex blanket flows.

Introduction. The goal of the paper is to introduce modeling approaches, which are being used at the Fusion Science and Technology Center at the University of California, Los Angeles, as applied to the so-called Dual Coolant Lead Lithium (DCLL) blanket of a fusion power reactor [1], to address various issues of MHD flows in a reactor strong magnetic field. At present the DCLL concept is considered in the US as a candidate for testing in ITER and for using in the next DEMO reactor.

In the DCLL blanket, the self-cooled breeder, Pb-17Li, circulates for power conversion and tritium breeding, experiencing MHD effects. Reduced activation ferritic steel is used as a structural material. Helium is used to cool the fist wall and

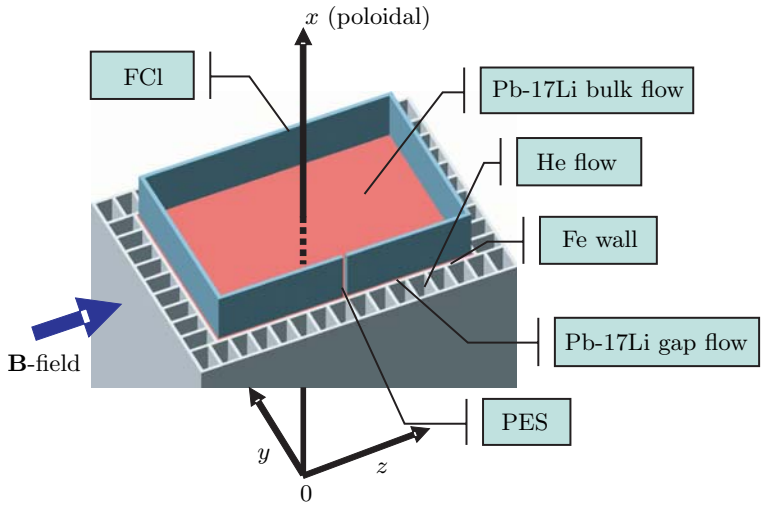

Fig. 1. Typical poloidal blanket channel with the FCI and helium cooling channels. The FCI has a slot (PES) to equalize the pressure on both sides of the insert.

Table 1. DCLL blanket channel parameters.

Poloidal length, L:	2 m	Ferritic wall thickness:	0.005 m
Toroidal width, $2b$:	0.3 m	PES width:	0.005 m
Radial depth, $2a$:	0.2 m	Magnetic field (outboard), B_z^0:	4 T
FCI thickness:	0.005 m	Pb-17Li flow velocity, U_0:	0.06 m/s
Gap width:	0.002 m	Inlet Pb-17Li temperature:	460°C

the blanket structure. A typical blanket channel is shown in Fig. 1. A key element of the concept is the flow channel insert (FCI) made of a silicon carbide composite (SiC_f/SiC), which is used as an electric insulator to reduce the impact from the MHD pressure drop, and as a thermal insulator to separate the high temperature Pb-17Li from the ferritic structure. The FCI is separated from the wall by a thin gap filled with the same liquid metal. The same pressure head drives the liquid metal through the channel and the gap. There can be openings in one of the walls of the FCI, such as a pressure equalization slot (PES), to equalize the pressure on both sides of the FCI, thus resulting in almost no primary stresses in the insert. The basic channel dimensions and other related parameters under the US DEMO reactor conditions are summarized in Table 1. The most important dimensionless parameters are the Reynolds number, $\mathrm{Re} = U_0\, b/\nu$, and the Hartmann number, $\mathrm{Ha} = B_z^0\, b(\sigma/\nu\rho)^{0.5}$, defined by the mean bulk velocity U_0, toroidal magnetic field B_z^0, half of the channel width b, and physical properties of the liquid: density ρ, electric conductivity σ, and kinematic viscosity ν. In the reference blanket flow, $\mathrm{Ha} = 15,900$ and $\mathrm{Re} = 83,700$.

The paper considers MHD effects in the poloidal flow. A fully developed flow model, including turbulence, along with the numerical code and calculation results are presented in Section 1. Initial results on modeling buoyancy effects are introduced in Section 2. Section 3 discusses the newly-developed MHD software, called HIMAG, which potentially can be used as a numerical tool for simulating complex geometry blanket flows.

1. Fully developed flow with the FCI. A mathematical model for a fully developed flow in the blanket channel (Fig. 1) in a toroidal magnetic field, B_z^0, is formulated in terms of the flow velocity U and the induced magnetic field B_x:

$$\frac{\partial}{\partial z}\left[(\nu+\nu_{tz})\frac{\partial U}{\partial z}\right]+\frac{\partial}{\partial y}\left[(\nu+\nu_{ty})\frac{\partial U}{\partial y}\right]-\frac{1}{\rho}\frac{\mathrm{d}P}{\mathrm{d}x}+\frac{B_z^0}{\rho\mu_0}\frac{\partial B_x}{\partial z}=0\,; \qquad (1)$$

$$\frac{1}{\mu_0}\frac{\partial}{\partial z}\left(\frac{1}{\sigma_y}\frac{\partial B_x}{\partial z}\right)+\frac{1}{\mu_0}\frac{\partial}{\partial y}\left(\frac{1}{\sigma_z}\frac{\partial B_x}{\partial y}\right)+B_z^0\frac{\partial U}{\partial z}=0\,. \qquad (2)$$

The model incorporates anisotropy in electric conductivity of SiC_f/SiC and turbulence. Eq. (1) is applied to the liquid domain, including the bulk flow region and the gap, while Eq. (2) covers the whole domain shown in Fig. 1. Eq. (2) is written in a conservative form. Thus, inner boundary conditions on B_x at the interfaces are not needed. Only the outer boundary condition in the form of $B_x = 0$ is formulated at the external surface of the ferritic wall.

1.1. Laminar flow. First, computations were performed assuming the flow to be laminar ($\nu_t = 0$). A finite-volume, conservative, collocated mesh code [2] was applied to Eqs. 1 and 2 in the multi-material domain shown in Fig. 1. The

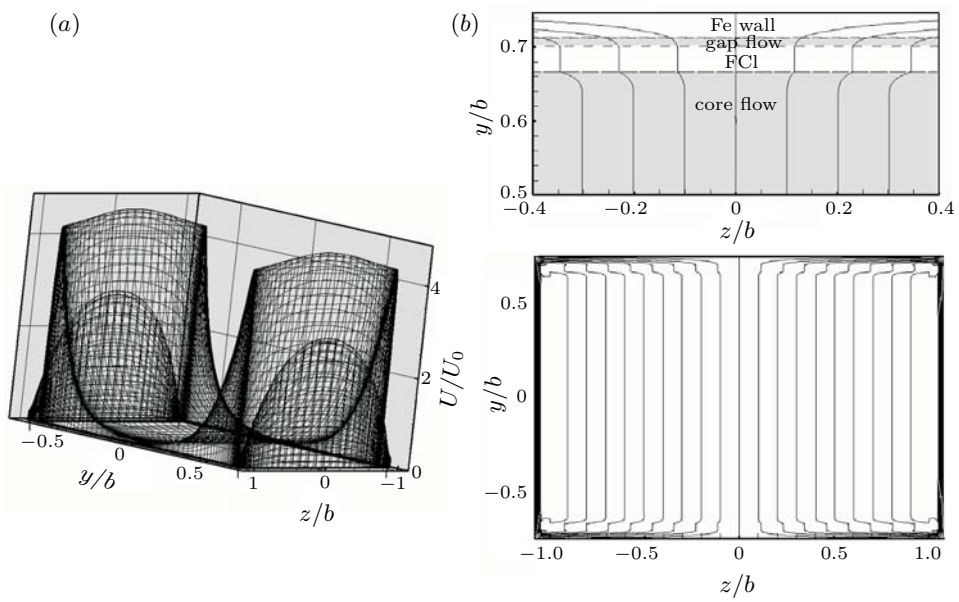

Fig. 2. Typical poloidal blanket channel with the FCI and helium cooling channels. The FCI has a slot (PES) to equalize the pressure on both sides of the insert.

code includes automatically generated Hartmann number sensitive meshes and effective convergence acceleration technique. Tests performed at Ha $\sim 10^4$ showed a very good accuracy. The electric conductivity of the SiC composite depends on the fabrication technique, neutron irradiation and many other factors. The computations were performed in a parametric form for $\sigma_{\mathrm{SiC}} = 5$–$500$ S/m. One computation takes from a few hours to three days with a PC at a 250×250 grid. Illustrations are shown for three cases: no openings in the FCI; PES in the side wall; and PES in the Hartmann wall. Here we use terms "Hartmann" and "side" for the walls perpendicular and parallel to the magnetic field.

A typical velocity profile and an induced magnetic field distribution in the case with no pressure equalization openings are shown in Fig. 2. The electric current induced in the core of the bulk region crosses the side FCI walls in the normal direction. After leaving the FCI, the electric current turns at almost 90° and flows tangentially through the gap and the wall. A characteristic feature of the flow is two high velocity jets near the side walls, which carry most of the volumetric flow rate. Appearance of the near-wall jets is a typical manifestation of the MHD effects in electrically conducting ducts or ducts with imperfect insulation. Many examples of "M-type" velocity profiles and explanations for the mechanism of the jet formation can be found in the MHD literature (e.g., [3]). Special numerical and asymptotic analysis for ducts with thin insulating coatings, also showing the jet flows, was performed in [4]. It is noticeable that the present analysis shows significant differences in the flow in the two different sections of the gap. In the side gap, where the electric current is mostly parallel to the magnetic field, the velocity is comparable with the near-wall jets, and the velocity profile is close to parabolic. In the Hartmann gap, the velocity is of a Hartmann type, and the flow is almost stagnant. As the electric conductivity of the silicon carbide composite decreases, the effect of electromagnetic coupling between the flow in the gap and the bulk flow reduces; the velocity in the gap drops relative to the mean velocity in the bulk region (Fig. 3*a*, *b*). One can also observe a strong reduction of the

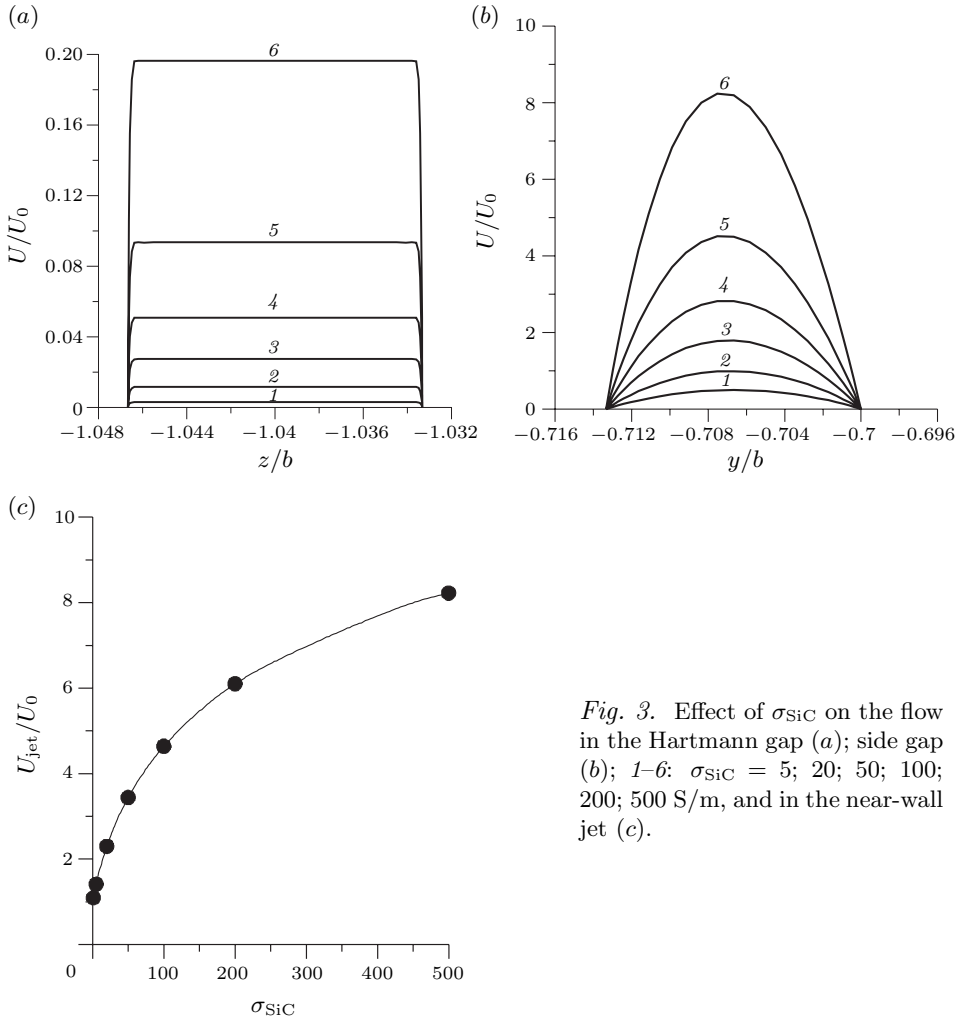

Fig. 3. Effect of $\sigma_{\rm SiC}$ on the flow in the Hartmann gap (*a*); side gap (*b*); *1–6*: $\sigma_{\rm SiC}$ = 5; 20; 50; 100; 200; 500 S/m, and in the near-wall jet (*c*).

near-wall jets (Fig. 3*c*). However, even at $\sigma_{\rm SiC}$ = 5 S/m the jet flow still exists, showing that the FCI is not a perfect insulator.

In the case with the pressure equalization slot in the Hartmann wall, all major flow features observed in the case with no openings, such as near-wall jets, are essentially the same. The main differences are local and occur within a narrow area adjacent to the slot (Fig. 4). In this area, the induced magnetic field contour lines are slightly disturbed, and the velocity profile exhibits a velocity deficit zone, stretching from the wall with the slot at $z = -b$ to the opposite Hartmann wall.

In the case with the pressure equalization slot in the side wall, the electric currents flow mostly through the slot, which exhibits a lower electric resistance than the FCI (Fig. 5). In the slot, the electric current flows perpendicular to the magnetic field lines, resulting in a strong flow-opposing Lorentz force, which turns the flow in the slot region in the opposite direction. The slot also affects the near-wall jet, which is sufficiently reduced if compared to the other jet at the opposite wall, which seems not to be affected by the slot. However, in practice, the reverse flow most likely will be modified by a convective motion. As the electric conductivity of the FCI decreases, the reverse flow in the near-slot area decreases.

1.2. Turbulent flow. In a strong reactor magnetic field, turbulence is anisotropic, demonstrating 2-D features. The turbulent structures appear as columnar

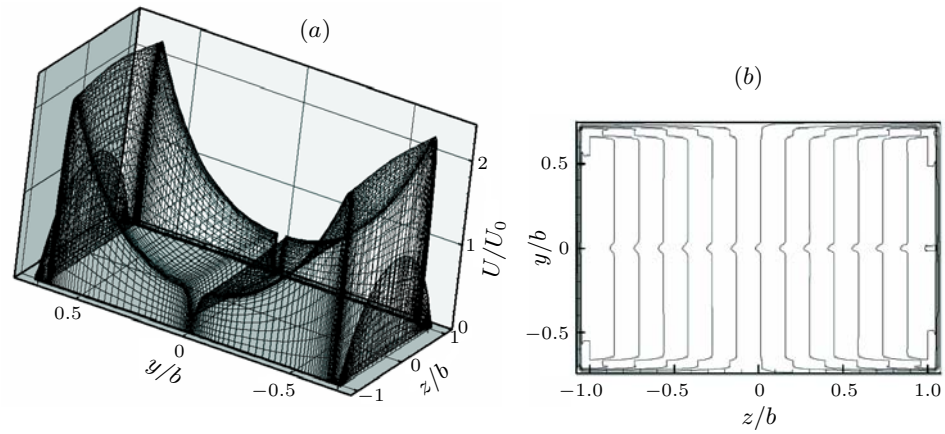

Fig. 4. Velocity distribution (a) and induced magnetic field contour plot (b) in the flow with PES in the Hartmann wall of the FCI at $\sigma_{\mathrm{SiC}} = 20$ S/m. The PES is located at $z = -b$.

vortices with their axis aligned in the magnetic field direction. The turbulence production is associated with the internal shear layers, while the dissipation mechanism is mostly related to viscous and ohmic losses in the Hartmann layers. To describe the highly anisotropic MHD turbulence, a closure relation is needed for ν_{ty}, while $\nu_{tz} = 0$. The turbulent viscosity was obtained by equating a shear layer thickness derived analytically for a simple shear flow to the shear layer thickness from the MATUR experiment [5]:

$$\frac{\nu_{\mathrm{t}}}{\nu} = C\frac{a}{b}\,\mathrm{Re}_*\big[1 - \exp\big\{-\sqrt{\mathrm{Ha}}(a/b - |y/b|)\big\}\big]. \tag{3}$$

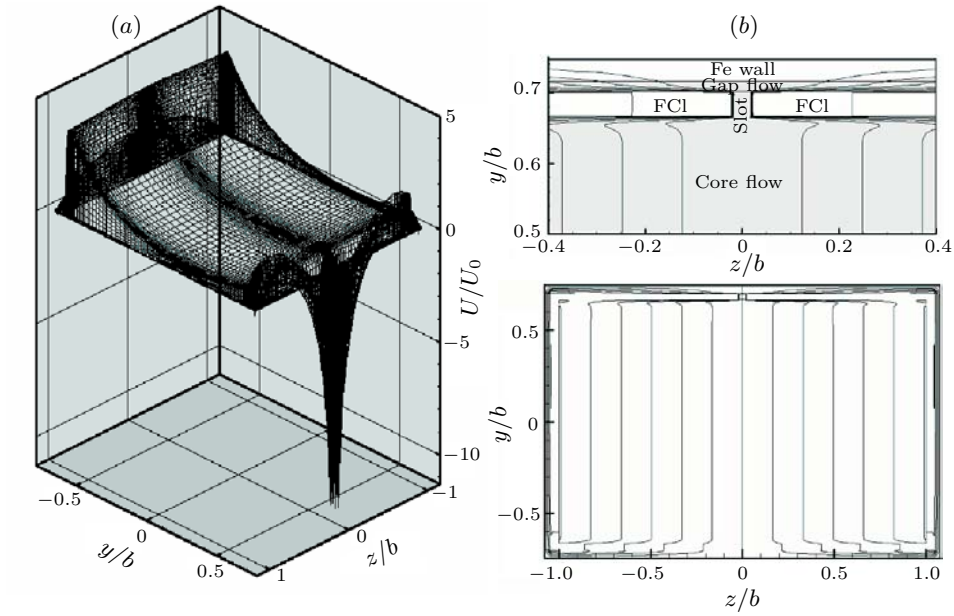

Fig. 5. Velocity distribution (a) and induced magnetic field contour plot (b) in the flow with PES in the side wall of the FCI at $\sigma_{\mathrm{SiC}} = 20$ S/m.

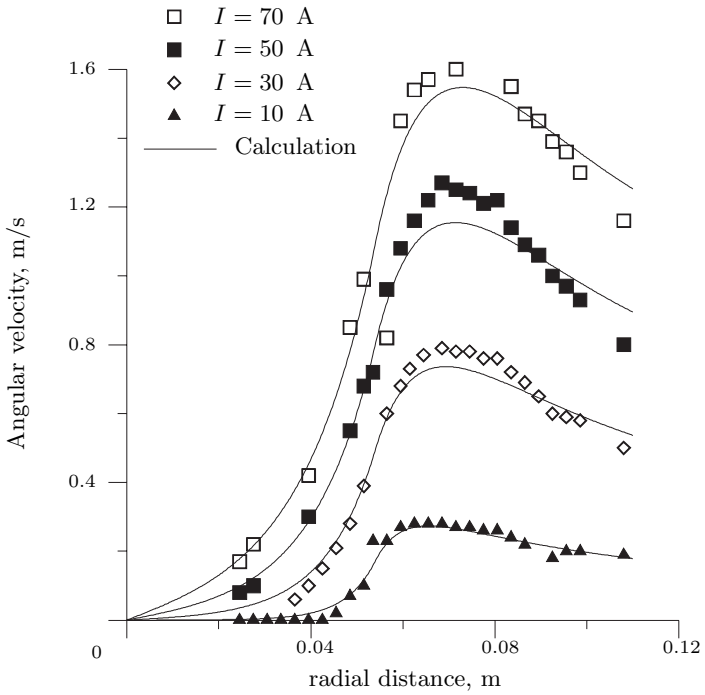

Fig. 6. Comparison of the calculations based on the zero-equation turbulence model with the experimental data obtained in the MATUR experiment ($B = 5\,\mathrm{T}$) [5].

In Eq. (3), Re_* is constructed from the characteristic velocity difference, $U_* = U_{\max} - U_{\min}$ in the flow domain and C is an empirical constant. An exponential correction (a wall function) was introduced to suppress the turbulence production at the side walls, where the flow is supposed to be laminar. First, the model was verified against experimental velocity profiles measured in the MATUR experiment (Fig. 6), where a turbulent shear in a cylindrical layer of mercury was driven by applying an electric current and a magnetic field. Then, calculations were performed for the reference blanket flow with the FCI without openings (Fig. 7). One can see a strong reduction of the near-wall jets in about 3 times due to turbulence diffusion (compare with the laminar case in Fig. 2). At the same time, the flow in the gap remains laminar; the maximum velocity in the side gap is significantly higher than that in the bulk flow. Unlike a laminar flow, the electric current lines in the bulk of the turbulent flow are not straight. The MHD pressure drop in the turbulent case is only slightly above the laminar value, indicating that the friction component of the pressure drop is much smaller than that due to the Lorentz force. A strong effect of turbulence on heat transfer can be predicted from the reduction of the near-wall jets and due to the increase of the effective thermal conductivity, which is (in the reference flow) by a factor of 10.

2. Buoyancy effects. The buoyancy effects on the flow and heat transfer are modeled in the Boussinesq approximation on the basis of a quasi-2D model for MHD flows in a non-conducting channel in a strong uniform magnetic field, known as the SM82 model [6]. The equations are formulated in terms of the vorticity $\omega = \partial V/\partial x - \partial U/\partial y$ and stream function ψ ($U = \partial\psi/\partial y$; $V = -\partial\psi/\partial x$):

$$\frac{\partial\omega}{\partial t} + U\frac{\partial\omega}{\partial x} + V\frac{\partial\omega}{\partial y} = \nu\left(\frac{\partial^2\omega}{\partial x^2} + \frac{\partial^2\omega}{\partial y^2}\right) - \frac{1}{\mathrm{Ha}}\frac{\nu}{b^2}\omega - g\beta\frac{\partial T}{\partial y}; \qquad (4)$$

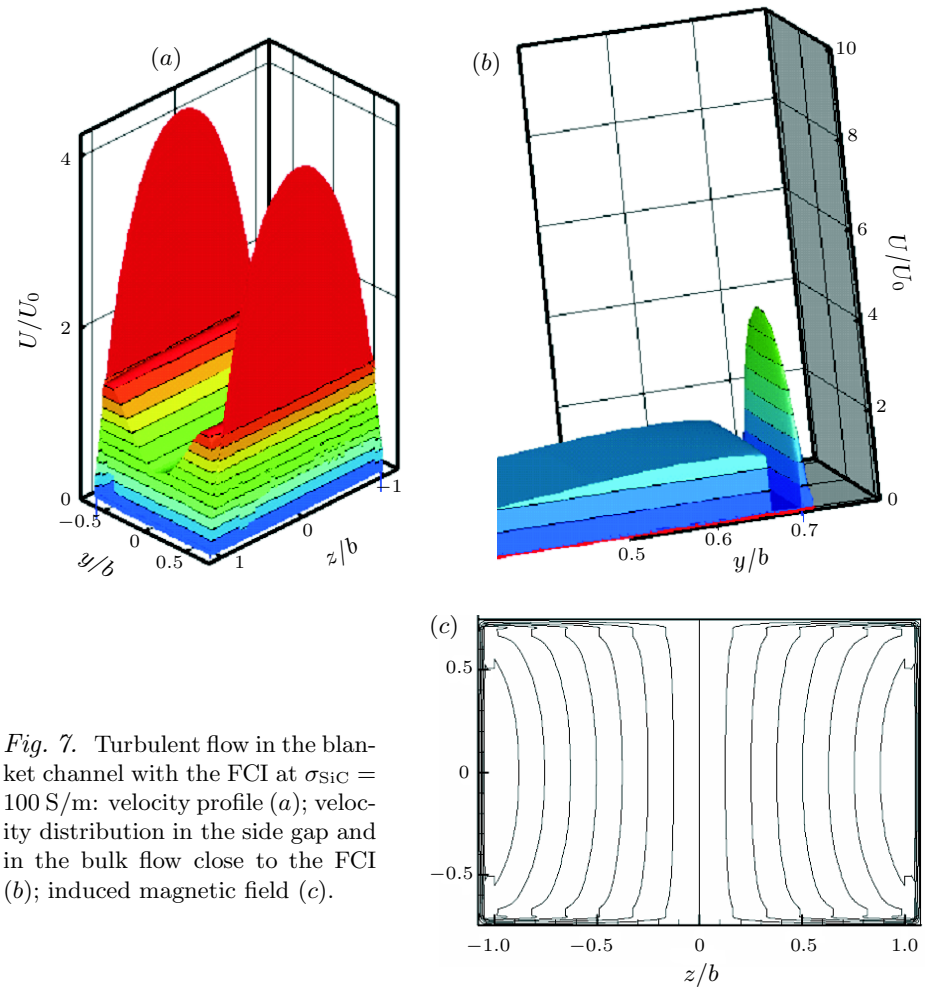

Fig. 7. Turbulent flow in the blanket channel with the FCI at $\sigma_{\mathrm{SiC}} = 100$ S/m: velocity profile (a); velocity distribution in the side gap and in the bulk flow close to the FCI (b); induced magnetic field (c).

$$\frac{\partial^2 \psi}{\partial x^2} + \frac{\partial^2 \psi}{\partial y^2} = \omega; \tag{5}$$

$$\rho C_{\mathrm{p}} \left(\frac{\partial T}{\partial t} + U \frac{\partial T}{\partial x} + V \frac{\partial T}{\partial y} \right) = k \left(\frac{\partial^2 T}{\partial x^2} + \frac{\partial^2 T}{\partial y^2} \right) + q'''. \tag{6}$$

All variables in Eqs. (4)–(6) are averaged via integration of the original 3-D equations along the magnetic field lines. The source term in Eq. (6) stands for the volumetric heat generated in Pb-17Li by neutrons. It is determined independently on neutronics calculations, where the detailed radial build is modeled using the neutron and gamma transport code DANTSYS [7]. The neutronics results for the radial variation of nuclear heating are then approximated as a function of the radial depth in the following form:

$$q''' = q_0 \, \mathrm{e}^{-(y+a)/l}. \tag{7}$$

Typical magnitudes of the parameters in Eq. (7) for the DEMO reactor at the outboard are: $q_0 = 30$ MW/m^3 and $m = a/l = 1$. Some results for the flows described by Eqs. (4)–(7) are shown below for pure natural and mixed convection regimes.

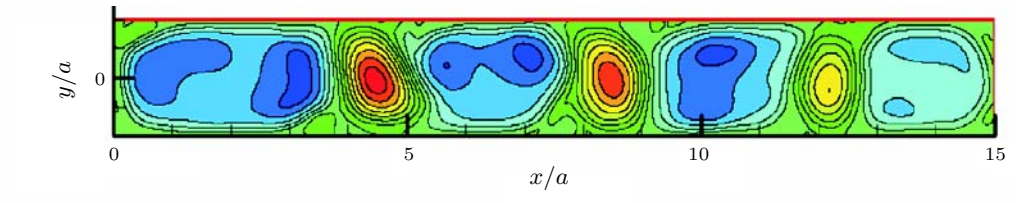

Fig. 8. Streamfunction contour plot for the natural convection flow: $\mathrm{Gr} = 0.5 \times 10^7$, $\mathrm{Ha} = 50$.

2.1. Pure natural convection. A number of tests was performed to benchmark a recently developed 2D unsteady code for solving Eqs. (4)–(6) against the numerical results presented in [8]. To match the cases in [8], differential heating and no volumetric heat were assumed first. Special attention was paid to the approximation of the convective terms, since the flow under the blanket conditions can demonstrate turbulent features (despite the magnetic field is strong). At present, three different approximations of the convective terms are tested: a Samarsky scheme (second-order upwind scheme with compensation of the schematic viscosity), a central-difference scheme, and a conservative Arakawa approximation. The results of computations for a pure natural convection case, using the same flow parameters, Grashof ($\mathrm{Gr} = g\beta a^3 \Delta T/\nu^2$) and Prandtl ($\mathrm{Pr} = \nu/\alpha$) numbers, as described in [8], are shown in Fig. 8. Present calculations agree well with the results in [8], demonstrating similar cell-type structures and the same value of the Nusselt number. Computations for poloidal flows in the blanket with volumetric heating, using the same approach, are in progress.

2.2. Mixed convection. The liquid is heated volumetrically. The boundaries $y = \pm a$ are thermally insulated. The flow velocity at the inlet is U_0. The problem is described by Eqs. (4)–(6). If the channel is long enough, a fully developed flow regime can be established. In the fully developed regime $V = 0$, $U = U(y)$, and the temperature field can be written as $T(x, y,) = T_0 + \gamma x + \theta(y)$. The original problem can be reduced to two ODEs:

$$\nu U'' - \frac{\nu \mathrm{Ha}}{b^2} U + g\beta\theta = -G\,; \tag{8}$$

$$\gamma U - \frac{k}{\rho C_\mathrm{p}} \theta'' = \frac{q_0}{\rho C_\mathrm{p}}\, \mathrm{e}^{-(y+a)/l}\,. \tag{9}$$

Here, G and γ are two constants, which are defined from the global energy/mass balance. The other notations are standard. In a strong magnetic field, the side layers are thin $\sim 1/\mathrm{Ha}^{1/2}$. The flow rate in the side layers is small. Thus, the problem can be solved in the core flow approximation, by neglecting the second order derivative in Eq. (8). The solution for the core variables is:

$$\theta(y) = \frac{q_0 a^2}{k} \left\{ \frac{m/r}{r^2 - m^2} \left[\frac{\mathrm{e}^{-2m} \cosh[r(y/a+1)] - \cosh[r(y/a-1)]}{\sinh(2r)} \right] + \right.$$
$$\left. + \frac{\mathrm{e}^{-m(y/a+1)}}{r^2 - m^2} - \frac{1 - \mathrm{e}^{-2m}}{2m} \frac{1}{r^2} \right\}; \tag{10}$$

$$U(y) = U_0 \Big[1 + r^2 \frac{k}{q_0 a^2} \frac{2m}{1 - \mathrm{e}^{-2m}}\, \theta(y) \Big]; \tag{11}$$

$$r = \sqrt{\frac{1 - \mathrm{e}^{-2m}}{2m} \frac{\mathrm{Gr}_*}{\mathrm{Ha}\,\mathrm{Re}(a/b)^2}}. \tag{12}$$

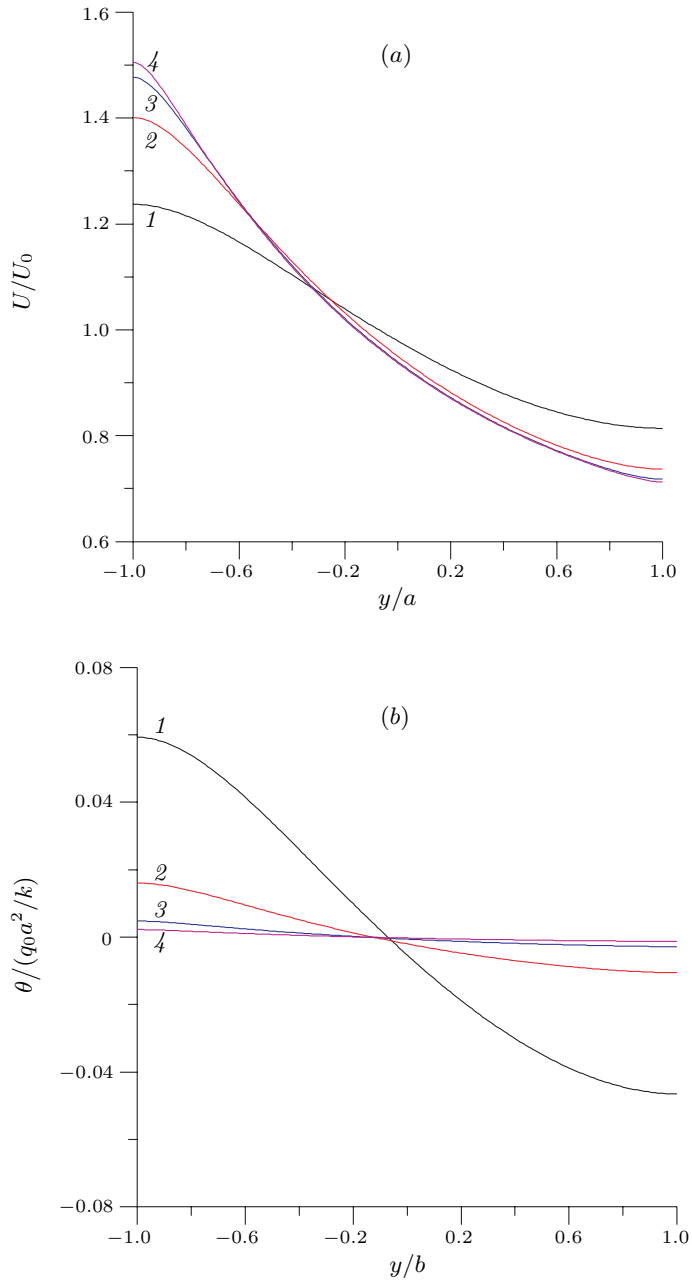

Fig. 9. Velocity (a) and temperature (b) in the mixed convection flow. $r = 2$ (*1*), 5 (*2*), 10 (*3*), 15 (*4*).

Here $\mathrm{Gr}_* = g\beta q_0 a^5/(\nu^2 k)$ is the modified Grashof number, and $\mathrm{Re} = U_0 a/\nu$ is the Reynolds number. It is noticeable that all dimensionless parameters are integrated into one, r. For the reference blanket flow, $r \sim 10^2$. Solution (10)–(12) suggests flattening of the temperature distribution but sufficiently different velocities at the opposite walls (Fig. 9). The distributions demonstrate an asymptotic behaviour for r. However, fully developed flows have not been observed in the numerical computations, since the blanket channel is not long enough, and vortex generation

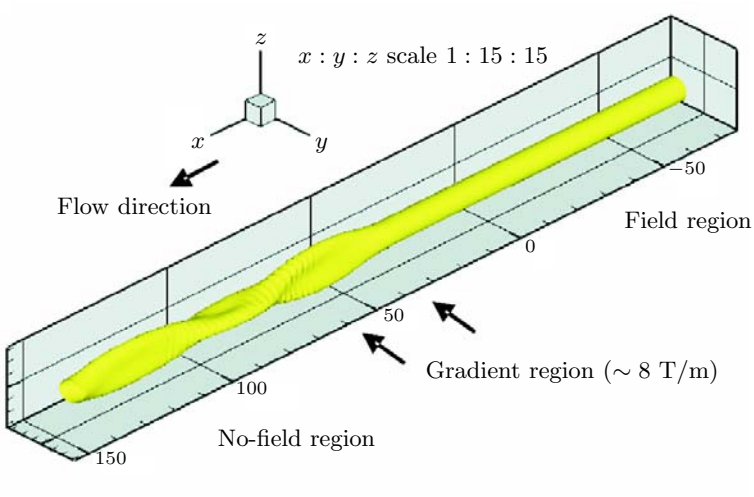

Fig. 10. Li jet with Re = 5000, Ha = 100, passing through the fringing field. The jet flattens and then oscillates due to capillary forces.

occurs in the shear layers, making the flow much more complex.

3. HIMAG code. Only a few attempts have been known to develop a 3D software for high Hartmann number MHD flows [9, 10]. The HyPerComp Incompressible MHD Solver for Arbitrary Geometry (HIMAG) is under development over the past several years at a US software company named HyPerComp, with some support from UCLA [11]. At the beginning of the code design, the emphasis was on the accurate capture of a free surface in low to moderate Hartmann number flows, such as jet and open-channel flows under laboratory or experimental reactor conditions. To pursue this goal, an unstructured grid formulation was utilized to allow any geometry of the fluid flow, nozzles, obstructions, *etc.*, and to provide adequate resolution of thin MHD boundary layers. Parallel solver implementation was used to allow large problem sizes to be solved in an acceptable amount of time. A second-order level set method was applied for tracking the free surface. Tests were performed for free surface flows to validate the code under various conditions [12], demonstrating a reasonable accuracy. A typical free surface simulation, showing the flattening of a lithium jet passing through a fringing magnetic field, is illustrated in Fig. 10.

At present, efforts are directed to the code modification and benchmarking for higher Hartmann number flows in typical closed channel configurations relevant to the DCLL blanket. The present version of the code includes:

- 3D incompressible flow solver (2D-order accurate in space and time);
- finite volume discretization on unstructured meshes using collocated arrangement (all unknowns are located at the cell centers);
- electric potential formulation with a possibility to simulate the induced currents closing-in through solid walls of a conducting channel;
- four-step projection method with semi-implicit Crank–Nicholson formulation for the convective and diffusion terms;

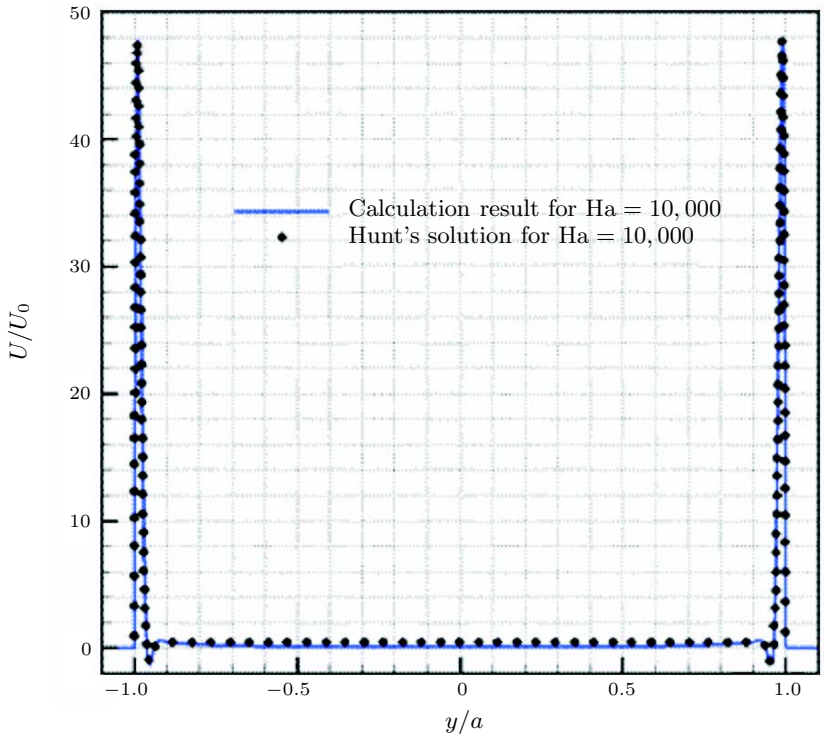

Fig. 11. Comparison of HIMAG calculations with the analytical solution [13] for a fully developed rectangular channel flow (Hartmann walls are conducting) at Ha = 10, 000.

- multiple strategies to account for mesh skewness;
- parallel architecture using computational clusters;
- graphical user interface.

Besides the development of the solver, a significant effort is proceeding to develop an alternate approach based on the induced magnetic field, to implement semi-analytical treatment of the Hartmann layers and to include models for buoyancy effects and turbulence. Current testing is underway to check the code validity for flows with either cross-sectional or axial currents using available analytical solutions, experimental data and results computed by other codes. The present benchmarks show a reasonable accuracy when the code is applied to high Hartmann number flows for relatively simple geometries (Fig. 11). Validations and the above-mentioned improvements of the code for complex geometry flows are still required.

Acknowledgements. We acknowledge the contribution of HIMAG developers, M.-J. Ni (UCLA) and the HyPerComp team. We are grateful to M. Sawan (University of Wisconsin) for neutronics calculations.

REFERENCES

[1] M. Abdou *et al.* US Plans and Strategy for ITER Blanket Testing. In 16^{th} *ANS TOFE Meeting* (Madison, Sept. 14-16, 2004).

[2] S. Smolentsev, N.B. Morley, M. Abdou. Code development for analysis of MHD pressure drop reduction in a liquid metal blanket using insulation technique based on a fully developed flow model. *Fusion Eng. Des.*, vol. 73 (2005), pp. 83–93.

[3] R. Moreau. *Magnetohydrodynamics* (Kluwer, 1990).

[4] L. Bühler, S. Molokov. Magnetohydrodynamic Flows in Ducts with Insulating Coatings. *KfK 5103*, January 1993.

[5] K. Messadek, R. Moreau. An experimental investigation of MHD quasi-two-dimensional turbulent shear flows. *JFM*, vol. 456 (2002), pp. 137–159.

[6] J. Sommeria, R. Moreauu. Why, how and when MHD turbulence becomes two-dimensional? *JFM*, vol. 118 (1982), pp. 507–518.

[7] R.E. Algouffe *et al.* DANTSYS 3.0, A Diffusion Accelerated Neutral Particle Transport Code System. *LA-12969-M*, Los Alamos National Laboratory, June 1995.

[8] G. Authie, T. Tagawa, R. Moreau. Buoyant flow in long vertical enclosures in the presence of a strong horizontal magnetic field. Part 2. Finite enclosures. *Europ. J. Mech. B*, vol. 22 (2003), pp. 203–220.

[9] S. Aleksandrova, S. Molokov, C.B. Reed. Modeling of Liquid Metal Duct and Free-Surface Flows Using CFX. *ANL/TD/TM02-30*, June 2002.

[10] C. Mistrangelo, L. Bühler. Three-dimensional magnetohydrodynamic flows in sudden expansions. In *Proc. Joint 15^{th} Riga and 6^{th} Pamir International Conference on Fundamental and Applied MHD* (Riga, Latvia, June 27–July 1, 2005), vol. 1, pp. 239–242.

[11] R. Munipalli *et al.* Development of a 3-D Incompressible Free Surface MHD Computational Environment for Arbitrary Geometries: HIMAG. *DOE SBIR Phase-II Final Report*, June 2003.

[12] N.B. Morley *et al.* Progress on the modeling of liquid metal, free surface, MHD flows for fusion liquid walls. *Fusion Eng. Des.*, vol. 73 (2005), pp. 83–93.

[13] J.C.R. Hunt. Magnetohydrodynamic flow in rectangular ducts. *J. Fluid. Mech.*, vol. 21 (1965), pp. 577–590.

Received 05.05.2006